Research Square

Preprints are preliminary reports that have not undergone peer review.
They should not be considered conclusive, used to inform clinical practice,
or referenced by the media as validated information.

Continental-Scale Groundwater Storage Dynamics and Climate Variability Across Africa (2003–2025): Regional Divergence and Hydro-Climatic Regime Shifts

Grmay Kassa Brhane
Academia Sinica
Chuen-Fa Ni
nichuenfa@geo.ncu.edu.tw
National Central University
Chian-Yi Liu
Academia Sinica

Article

Keywords: Africa, climate variability, continental scale, groundwater storage, groundwater response trend

Posted Date: November 9th, 2026

DOI: https://doi.org/10.21203/rs.3.rs-11268104/v1

License: This work is licensed under a Creative Commons Attribution 4.0 International License.
Read Full License

Additional Declarations: No competing interests reported.

Continental-Scale Groundwater Storage Dynamics and Climate Variability Across Africa (2003–2025): Regional Divergence and Hydro-Climatic Regime Shifts

Grmay Kassa Brhane[1,2], Chuen-Fa Ni[1*,2,3], Chian-Yi Liu[1,4,5]

[1]Earth System Science Program, Taiwan International Graduate Program, Academia Sinica, Taiwan

[1*]Graduate Institute of Applied Geology, National Central University, Taoyuan City, 32001, Taiwan, email: nichuenf@gmail.com, Corresponding Author

[2]Department of Earth Sciences, College of Earth Sciences, National Central University, Taoyuan City, 32001, Taiwan

[3]Center of Environmental Studies, National Central University, Taoyuan City, 32001, Taiwan

[4]Research Center for Environmental Changes, Academia Sinica, Taipei 11529, Taiwan,

[5]Center for Space and Remote Sensing Research, National Central University, Taoyuan 32001, Taiwan

Abstract: Groundwater is Africa's most important buffer against climate variability, yet its regional and continental response to climatic and anthropogenic drivers remains poorly quantified. The study integrates Gravity Recovery and Climate Experiment satellite gravimetry, Global Land Data Assimilation System land-surface model output, and surface water storage estimates in a mass-balance framework to derive the groundwater storage anomalies (GWSA), recharge, and discharge across Africa since 2003 on a common 0.25° regular grid, and to assess the GWSA response to precipitation, temperature, and ENSO to characterize its climate sensitivity. Results show that GWSA ranges from -30.60 mm (North Africa) to 96.56 mm (West Africa) at an overall trend of 3.84 mm yr^{-1} (precipitation 0.10 mm yr^{-1}). A formal structural break test identified a hydrodynamic shift in July 2020, with the GWAS trend rising from 2.59 to 5.74 mm yr^{-1}, coinciding with the onset of the 2020-2023 "triple-dip" La Niña. Recharge-to-precipitation ratio ranging from 11.0% to 21.5%, with regional GWSA trends of -0.78, 5.27, 5.12, 6.04, and 4.67 mm yr^{-1} trend of GWSA for North, West, Middle, East, and South Africa, respectively. This recovery continues even during the 2020-2022 Horn of Africa drought, underscoring GWSA's value as an indicator of climate and human influence, and the importance of regional variation for future water security assessments.

Keywords: Africa, climate variability, continental scale, groundwater storage, groundwater response trend

1. Introduction

As a massive and growing body of water, groundwater is the primary buffer for Africa's ecosystems, agricultural activities, and populations, particularly in climate-sensitive areas [1]. Recent research [2] found that, continentally, Africa has highly heterogeneous hydrological systems that are prone to both small-scale climatic disasters and global climate change. Recent research also shows that African aquifers are disproportionately important for absorbing multi-year climate extremes compared to other regions because of low groundwater exploitation rates and episodic recharge [3,4]. Nevertheless, climate-driven recharge variability is further aggravated by human activity, with shifts in land use, rising irrigation demands, and urbanization increasing the abuse of already depleted aquifers, which is expected to intensify [5]. These factors reveal the need to thoroughly analyze groundwater-climate interactions in a way that informs and guides effective adaptation strategies. Such climate whiplash affects not only water but also food security, and the hydrology of most of Africa's major river basins remains among the least understood on Earth [6].

The varied climate of Africa is dominated by multifaceted interactions such as the seasonal shift of the Intertropical Convergence Zone (ITCZ) and global-scale ocean-atmosphere oscillation developments such as El Niño-Southern Oscillation (ENSO) and the Indian Ocean Dipole [7]. These phenomena alter precipitation patterns across the continent, causing years of excessive rain and multi-year droughts. It is challenging to break down the total water storage signal to isolate the critical groundwater storage anomaly (GWSA) component, and it is essential to include additional data provided by land surface models [8]. Moreover, the GWSA reflects the contribution of natural and human-made components, which are both spatiotemporally dynamic factors, where the natural component is attributed to the fluxes of water balance related to the climate (precipitation, evapotranspiration, and other storage terms such as soil moisture, canopy water, snow, and surface water), while the anthropogenic component refers to the difference between the total observed GWSA and the natural component, representing the net effect of anthropogenic water-balance fluxes, including water abstraction [9].

In Africa, groundwater is the key buffer against hydrological variability, especially as climate extremes and populations continue to increase, alongside changes in land-use patterns. Recent studies [8,10] highlight the shift and how more groundwater is being relied on because surface water

is increasingly unreliable, and changes in land-use patterns, such as in West Africa, and water extraction are currently impacting recharge processes and influencing groundwater storage [11]. Groundwater resources in Africa at the continental scale remain poorly understood because of a scarcity of long-term, in situ monitoring data. Moreover, pressures on these resources are increasing rapidly due to population growth, economic development, and rising demand for irrigated agriculture to ensure food security [3]. This imbalance between rising demand and limited data for water management poses a major challenge to sustainable water management. Hence, a continental-scale study of the entire groundwater system response to climate anomalies and anthropogenic contributions to groundwater storage anomalies is a key information gap.

Groundwater monitoring networks are often sparse, unevenly distributed, and long-term in-situ records are incomplete and inaccessible, particularly in Africa, limiting the ability to assess groundwater on a continental scale [4,12]. This ongoing observational deficit has driven a shift toward satellite-based methods for assessing groundwater at large scales. The Gravity Recovery and Climate Experiment (GRACE) mission provides continental- to regional-scale estimates of terrestrial water storage anomalies that are continuous in space and time [13] and can be used to isolate groundwater storage from land surface model outputs such as the Global Land Data Assimilation System (GLDAS) [14]. This method has been applied to estimate groundwater storage changes in data-limited basins globally Gleeson et al., 2015) and over key aquifer systems in Africa to link groundwater storage variability to hydrologic extremes and climate teleconnections [10]. Other recent developments, such as singular spectrum analysis, have further enhanced the temporal continuity of GRACE-derived records across data gaps during the mission [15].

To address this continental-scale knowledge gap, the present study aims to quantify long-term changes in groundwater storage and their climatic drivers across regional and continental contexts in Africa (2003–2025) using GRACE-based mass balance and auxiliary hydrological data, and to provide essential insights for groundwater policy and management. GRACE data enable tracking terrestrial water storage anomalies at large scales [13]. Combining terrestrial water storage anomalies with land surface model outputs could isolate groundwater storage anomalies, providing extraordinary insights into long-term groundwater response to climate variability and dynamic anthropogenic influence. Motivated by the advantages of satellite-based observations, this work comprehensively analyzed and quantified groundwater fluxes and storage, linking them to their

climate drivers. The objectives of the study are to move beyond simple correlations by (1) quantifying the trends of the GWSA and recharge along with the precipitation trend in a regional and continental context from 2003 to 2025, (2) linking the groundwater system's response to specific, documented climate extremes such as ENSO, and (3) linking the GWSA and recharge to the annual renewable groundwater resources trend at the continental level.

This study adopts the groundwater storage disaggregation method developed by Ferreira [16] based on the ensemble Kalman filter (EnKF). The processing steps have been adapted selectively according to the nature of the GRACE data product and the scientific goal of this study, which is quantifying groundwater storage and recharge and analyzing the response trend to climate variability at regional and continental scales in Africa. In this study, we use CSR RL0603 mascon solutions; therefore, we apply an alternative resolution-harmonization procedure, and we present each issue discussed in the following sections.

2. Materials and Methods

2.1. Study Area

The study domain includes the African continent, ranging from 35° S to 38° N and 20° W to 55° E on a regular 0.25° grid box, which was later refined to the true continental boundary, using an administrative country boundary from Natural Earth at 50-m resolution, with the boundary broken into five sub-regions: North Africa, West Africa, Middle Africa, East Africa and South Africa, according to the United Nations M49 standard geoscheme (**Fig. 1a).**

It is important to recognize that the 0.25° grid employed throughout this study functions as a standardized interpolation framework for spatial harmonization and aggregation across datasets with varying native resolutions (such as GRACE mascons, GLDAS, and DAHITI), rather than reflecting the actual 0.25° spatial resolution of the underlying GRACE signal. The native resolution of the CSR RL0603M mascon solution is approximately 300 km at the equator, indicating that individual 0.25° pixels in this study are not independently resolved measurements but are instead smoothly interpolated values derived from a coarser underlying field. Therefore, all significant conclusions are made at the regional (UN M49 sub-region) and continental scales, where averaging many correlated 0.25° pixels within a much larger true GRACE footprint is

statistically justified. Pixel-level values are provided solely for visualization and spatial pattern depiction and are not independently interpreted at that resolution.

2.2. Data Type and Sources

Terrestrial water storage (TWS) anomalies were derived from the Gravity Recovery and Climate Experiment (GRACE) and its Follow-On mission (GRACE-FO) with level 3 data on monthly 0.25° × 0.25° gridded mass concentration (mascon) solutions (CSR RL0603) from the Center for Space Research (CSR) at the University of Texas at Austin from February 2003 to April 2026. Mascon solutions provide a higher signal-to-noise ratio than traditional spherical harmonic solutions by incorporating geophysical constraints during processing [19] and are a strong method for quantifying large-scale changes in TWS [17]. Global Land Data Assimilation System (GLDAS) soil moisture storage (SMS) output from the Noah Land Surface Model (LSM) at a 0.25° spatial resolution was used to disaggregate the TWS signal, with monthly LSM outputs subject to uncertainties and biases [8,14]. In Africa, surface water storage was derived from monthly water-level time series from 23 major lakes and reservoirs, which were retrieved from the database DAHITI, a new alternative to the ground-based gauge networks that are unable to measure water storage on Africa's surface water resources [6], and used multi-mission satellite radar altimetry [18]. We used water-level data, along with the areal extent of each water body (km^2) and its water-body type, to calculate water-level changes. To prevent temporal inconsistencies before arithmetic operations across variables, we interpolated or resampled all datasets onto a common monthly master time axis spanning January 2003 to April 2026. Table 1 summarizes the data used in this study, their native spatial and temporal resolutions, and their main reference sources.

Table 1. Data sources used in this study.

Dataset	Variable(s)	Resolution	Coverage	Reference
GRACE / GRACE-FO (CSR RL0603 Mascons)	Total water storage anomaly (TWS)	0.25 deg (mascon)	2003-2026 (with GRACE/GRACE-FO gap)	[17]
GLDAS-Noah v2.1	Soil moisture (4-layer), snow water equivalent, canopy water storage, evapotranspiration	0.25 deg	2003-2026	[14]
DAHITI	Lake water level anomaly (23 confirmed lakes)	Point / per-lake	2003-2026	[19]
HydroLAKES	Lake polygon geometry and surface area (static)	Vector polygon	Static	[20]
CHIRPS	Precipitation	0.05 deg (regridded to 0.25 deg)	2003-2026	[21]
Reanalysis Temperature	2 m air temperature	~2.5 deg (native)	2003-2026	NOAA Climate Prediction Center
Oceanic Nino Index (ONI)	ENSO state index	Scalar (basin-averaged)	2003-2026	NOAA Climate Prediction Center
Natural Earth (50 m)	Country/continent boundaries	Vector polygon	Static	Natural Earth (naturalearthdata.com)
Groundwater data	Annual renewable groundwater and groundwater-irrigated area	Time series data	2003-2022	FAO
WHYMAP	Groundwater recharge potential classification	Point/vector	Static	[22]

2.3. Data Processing and Analysis

All the data-processing activities are channeled through several stages, connected to each other (**Fig. 1b**).

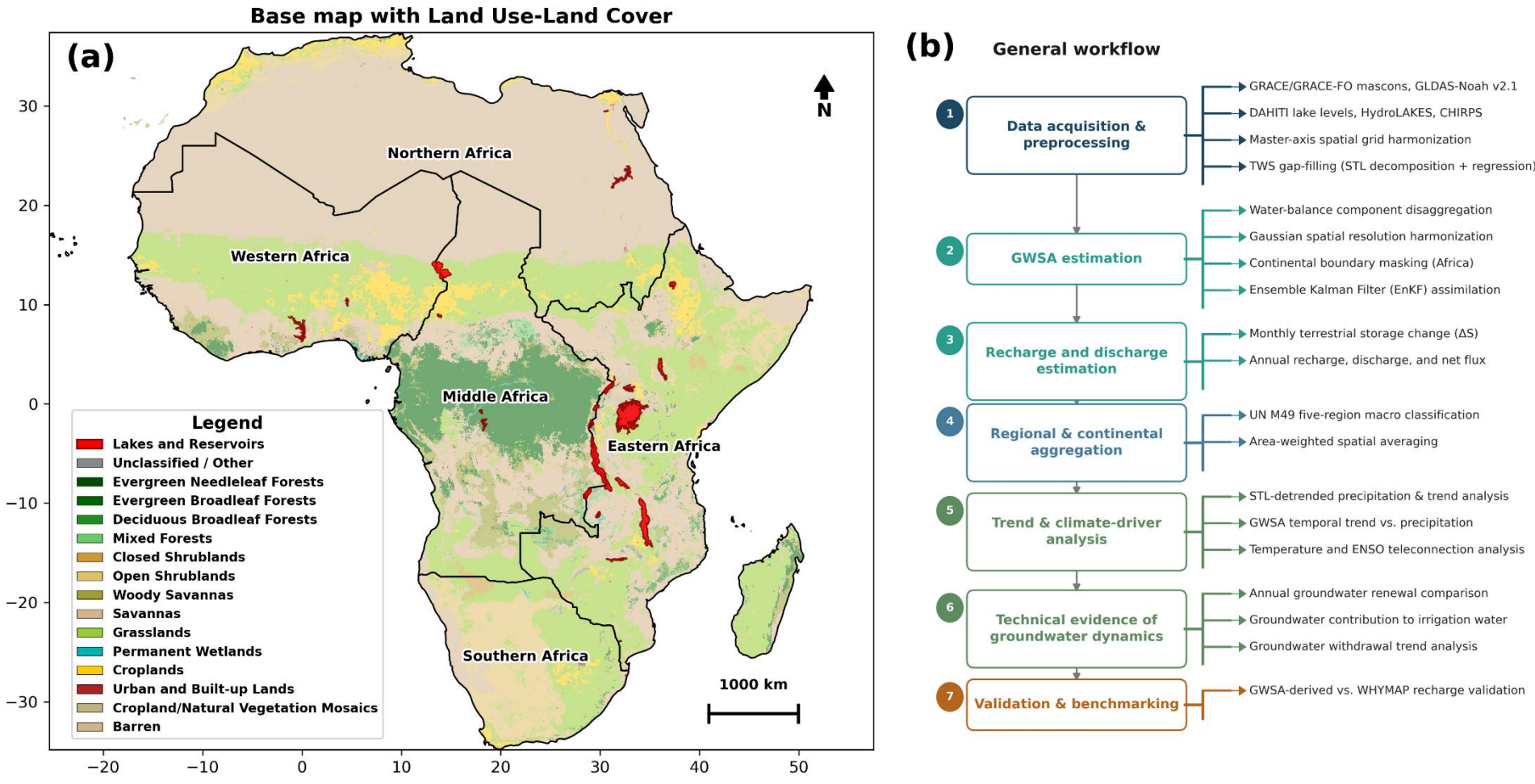


Fig. 1. Study area and data processing: a) Base map; b) General workflow

We first filled the GRACE data gap to create a continuous monthly GRACE record, then applied continental masking and harmonized resolution. In addition, all water-storage elements used were referenced to a common base period for anomaly production. We also computed the water-balance residual of total water storage (TWS) from the non-groundwater components (GW) at the grid level with 0.25-degree spatial resolution and passed it through the Ensemble Kalman Filter [16] to remove noise and retain the climatically relevant signal. Two analyses were conducted downstream of this filtered GWSA, including monthly groundwater fluxes and annual recharge/discharge derived directly from the filtered GWSA. All the data are processed at the grid level and aggregated to regional and continental scales. We performed seasonal trend decomposition of climate variables to obtain non-seasonal precipitation anomalies using independent precipitation datasets (CHIRPS), which have been analyzed and evaluated across various time scales (Huang et al., 2020; Liu et al., 2020). Furthermore, the trend analysis and quantification were performed for the GWSA, recharge, discharge, net recharge, precipitation, and temperature using the non-parametric Mann-Kendall test [23], applied at a continental-mean and regional-mean level, and then two independent climate indices, the Oceanic Niño Index (ONI) and surface temperature, were compared directly to GWSA to validate the physical reality of GWSA and quantify its sensitivity to large-scale climate teleconnections. Finally, validation of GWSA and recharge at regional and continental scales, as well as annual trend comparisons between GWSA and recharge and annual renewable groundwater resources at the continental scale, were performed, and computations and analyses were conducted using Python packages.

2.3.1 Lake Water-Level Data and Surface Water Storage

The DAHITI lake water-level anomaly time series[18] were matched with the HydroLAKES polygon database [20] and verified against the actual polygon geometry for physical plausibility, and 23 were retained after cross-checking with the actual HydroLAKES polygon geometry. To prevent the storage signal from a lake from artificially concentrating at one point, footprint anomalies over lakes with a footprint in several 0.25-degree grid boxes were spread across multiple grid boxes according to the portion of the lake polygon within each grid box. These volume anomalies were then gridded to the common 0.25-degree domain for the lake-scale SWR component, and volume anomalies were calculated for the lakes by applying the static-area approximation [16] equation (1):

$$\mathbf{\Delta Volume = Static_Area * \Delta h} \quad \textbf{(1)}$$

where Static_Area is the lake surface area, derived from the actual polygons from HydroLAKES, and Δh is the water-level anomaly calculated.

2.3.2. Filling Gap of GRACE Total Water Storage

The total water storage (TWS) record has a known break from the end of the first satellite mission to the beginning of the second (about 11 months, from 2017 to 2018). Linear interpolation [17] was used to complete short spans (scatterings) for interior gaps (3 months or less) in the record equation (**2**). The primary mission-transition gap was addressed by applying STL [24] to the pre- and post-gap TWS records, and the residual during the gap period was estimated by linear regression of the residuals of the observed TWS record equation (**3**).

$$\mathbf{TWS = TWS_1 * \frac{t-t1}{t2-t1} + TWS_2 * \frac{t2-t}{t2-t1}} \quad \textbf{(2)}$$

where TWS is missing at a specific time t in GRACE, TWS_1 and TWS_2 are TWS available at an earlier month, t1, and a later month t2 (t1 < t2).

$$\mathbf{Y_t = T_t + S_t + R_t} \quad \textbf{(3)}$$

where Y is the observed value at time t, T is the smoothly varying trend component, S is the periodic seasonal component, and R is the remainder. The decomposition uses STL (Cleveland et al., 1990), which is based on locally weighted regression and runs an iterative inner/outer-loop procedure: the inner loop alternates between seasonal and trend smoothing, and the outer loop applies robustness weights to reduce the impact of outliers.

2.3.3. Continental Masking and Resolution Harmonization

To avoid the propagation of non-African signals, most obviously the large total water storage signal such as the Caspian Sea in the north-east corner of the rectangular domain, all input components were masked to the true domain of Africa boundary (**Fig. 1a**), and truly African grid cells through the smoothing kernel were obtained. The Native 0.25-degree resolution results from direct application of equation (4) were found to produce physically unlikely extreme values at grid

cells corresponding to large lakes and along the boundary of the study domain due to the resolution mismatch between the true effective spatial resolving power of GRACE and the native resolution of the auxiliary GLDAS and lake-derived fields. Hence, all 5 water storage components in equation (4) were smoothed in space using Gaussian smoothing (as a mask-aware, latitude-dependent operation) before being disaggregated [25], as follows:

$$\mathbf{f'(x,y) = \frac{[\sum f(x_i,y_i)\cdot w_i]}{[\sum w_i],w_i} = exp(-d_i^2 \,/\, 2\sigma^2)} \quad \textbf{(4)}$$

where d_i is the great-circle distance between the grid cell i and the target location, σ is the smoothing radius, and the normalized-convolution form divides each value by the sum of the values of the unmasked valid cells to avoid bias in regions of data gaps and the coastal boundary [25].

To obtain a constant physical (km) smoothing radius, we adjusted the smoothing radius along each latitude row by varying the kernel width in the east-west direction to account for meridional convergence. The smoothing radius (σ) in equation (4) was not assumed beforehand; three candidate radii (100 km, 150 km, and 360 km) were tested, where the 360 km radius was found to be consistent in magnitude with [16], calculated for their own spherical-harmonic degree-55 truncation.

2.3.4. Determination of Groundwater Storage Anomaly (GWSA)

2.3.4.1. Terrestrial Water Storage (TWS) Disaggregation

Groundwater storage anomaly (GWSA) was estimated by disaggregating the TWS anomaly into the individual terrestrial water storage (TWS) compartments as follows [16]:

$$\mathbf{GWSA_t = TWS_t - [SWR_t + SMS_t + WSB_t + SIS_t]} \quad \textbf{(5)}$$

where TWS is total water storage anomaly, SMS is four-layer soil moisture storage anomaly (GLDAS-Noah), SIS is snow/ice storage anomaly (GLDAS snow water equivalent), SWR is surface-water storage anomaly, and WSB is canopy (vegetation) water storage anomaly (GLDAS canopy interception). Before disaggregation, all anomalies used a common 2004-2009 baseline period, and all terms represent monthly anomalies at 0.25-degree grid resolution in millimeters of equivalent water height.

2.3.4.2. Ensemble Kalman Filter Refinement

Once the resolution harmonization was done, the disaggregated GWSA was improved using an ensemble Kalman filter [16,26], and the forecast covariance for an ensemble of E members was calculated as follows:

$$\boldsymbol{P_f} = [\frac{\mathbf{1}}{(\boldsymbol{E-1})}] \sum _\mathbf{e} (\boldsymbol{x_e} - \bar{\boldsymbol{x}})(\boldsymbol{x_e} - \bar{\boldsymbol{x}})^{\mathbf{T}} \quad \textbf{(6)}$$

Then the Kalman K gain was determined as:

$$\boldsymbol{K} = \boldsymbol{P_f}\, H^{\mathbf{T}} \,(\, HP_f\, H^{\mathbf{T}} + \mathbf{R})^{-\mathbf{1}} \quad \textbf{(7)}$$

Furthermore, the updating of each ensemble member was as follows:

$$\boldsymbol{x_e}^{\mathbf{a}} = \boldsymbol{x_e}^{\mathbf{f}} + \mathbf{K}(\boldsymbol{y_e} - \mathbf{H}\boldsymbol{x_e}^{\mathbf{f}}) \quad \textbf{(8)}$$

Where, P_f, is the ensemble forecast covariance, calculated from the spread of the ensemble members at each grid cell and month, x_e is each of the E = 100 ensemble members, generated perturbing the disaggregated GWSA plus Gaussian noise with standard deviation 20 mm, $\bar{x}$ is the mean of the ensemble, H is the observation operator, taken as the identity matrix, as the observations of TWS are direct, R is the reported uncertainty in the GRACE TWS observations, set to 400 mm^2 (20 mm^2), and $\mathbf{y_e}$ is the perturbed observations, with each one being created with the same 20 mm uncertainty. $\boldsymbol{x_e}^{\mathbf{f}}$ and $\boldsymbol{x_e}^{\mathbf{a}}$ correspond to each ensemble member before and after the update, respectively. E, R, and H are based on the values and assumptions from the literature [16].

2.3.5. Estimation of Groundwater Fluxes (Recharge and Discharge)

The filtered monthly GWSA time series were used directly at the grid resolution to calculate effective annual groundwater recharge and discharge, and the monthly change in GWSA ($\Delta G'_t$) was estimated as follows [27,28]:

$$\mathbf{\Delta G_t} = \boldsymbol{G_t} - \boldsymbol{G_{t-1}} \quad \textbf{(9)}$$

Where G_{t-1} is the GWSA of the previous month, and G_t is the GWSA of the current month, for each month t. ΔG_t represents the net water gain or loss during that month. We calculated

continuous discharge (D_γ) and recharge (R_γ) for all months using methods from the literature [16,29].

The annual potential groundwater recharge (R_γ) was determined by summing all positive monthly changes over year **y** using equation (**10**) and represents the total groundwater gains.

$$\boldsymbol{R_\gamma = \sum max(\Delta G_t,\ 0)} \quad \textbf{(10)}$$

The Annual Discharge (D_y) indicates the loss of groundwater, which is the sum of the absolute values of all negative changes over the year

$$\boldsymbol{D_\gamma = \sum min(\Delta G_t,\ 0)} \quad \textbf{(11)}$$

The Net Annual Recharge is the difference between the two (R_γ - D_γ), and for each year, the total annual discharge is subtracted from the total annual recharge, resulting in the final balance between total annual gains and losses, which is equivalent to the net change in groundwater storage over that year [16,30]:

$$\mathbf{R_{net,\gamma} = R_\gamma - D_\gamma} \quad \textbf{(12)}$$

In mathematical terms, this is the same as deducting the storage level at the start of the year from the storage level at the year's conclusion. This analysis included a calendar year only if it contained ten of the twelve months with valid data; years with fewer than ten months were deemed invalid rather than imputed from partial data.

The uncertainty in the recharge and discharge estimates was assessed by propagating the ensemble standard deviation from the Ensemble Kalman Filter (EnKF), which was computed separately for every grid cell and month by calculating the spread in the 100-member updated ensemble. The mean monthly storage-change (ΔS) uncertainty was 19.9 mm, and the mean annual recharge/discharge uncertainty was ±69.1 mm yr^{-1} due to the ensemble spread being assumed to be independent between months, with the continental-average EnKF uncertainty of 14.1 mm. This represents about 53–123% of the recharge estimates in this region from storage changes derived from GRACE, which range from 56–130 mm yr^{-1}, and thus demonstrates that recharge estimates from GRACE-derived storage changes are still highly uncertain at annual timescales, even before

accounting for structural uncertainties in the disaggregation method itself (e.g. assumptions that the GLDAS and DAHITI provide a good representation of soil moisture, snow/ice and surface water storage changes). The uncertainties we have highlighted highlight the need for regionally and continentally validated classification against WHYMAP and ground-based estimates from MacDonald [4] below to assess the reliability of these recharge estimates outside of their nominal precision derived from the ensemble.

2.3.6. Regional and Continental Aggregation

The regional aggregation was done based on the five UN M49 sub-regions, where the continental and regional-scale time series were computed as area-weighted spatial averages, with each grid cell weighted by its true geodetic surface area:

$$\boldsymbol{A(\varphi)} = \mathbf{R_e^a} * \boldsymbol{\Delta\lambda} * [\boldsymbol{sin}([(\frac{\boldsymbol{\varphi+\Delta\varphi}}{\mathbf{2}}) - \mathbf{sin}((\frac{\boldsymbol{\varphi-\Delta\varphi}}{\mathbf{2}})] \quad \textbf{(13)}$$

where R_e is the radius of Earth (6371.0088 km), φ is cell-center latitude, and Δλ and Δφ are the grid-cell dimensions in radians (rather than a simple grid-cell count that would bias up poles).

2.3.7 Groundwater Response to Climate Variability

2.3.7.1 Long-term Trend Detection

The non-parametric Mann-Kendall test [23] was used to quantify trends in GWSA, recharge, discharge, net recharge, and precipitation, applied at a continental-mean and regional-mean as follows:

$$\mathbf{S} = \sum(\boldsymbol{i} < \boldsymbol{j})\mathbf{sgn}(\mathbf{X_j} - \mathbf{X_i}) \quad \textbf{(14)}$$

Where X_i and X_j are data points in the time series data of GWSA, recharge, discharge, net recharge, and precipitation at a position i (earlier) and j (later), S is asymptotically normal for n > 10, allowing for a standard z-test for trend significance.

These include the Theil-Sen slope estimator [23], which is asymptotically normal for n > 10 and allows for a standard z-test for trend significance, in addition to:

$$\boldsymbol{\beta} = \boldsymbol{median}[\frac{\boldsymbol{X_j - X_i}}{\mathbf{j-i}}], \textbf{for all i} < \textbf{j} \quad \textbf{(15)}$$

where $\boldsymbol{\beta}$ is the Theil-Sen slope, the median of all pairwise slopes $(x_j-x_i)/(j-i)$, which is the trend value for GWSA, precipitation, and temperature.

2.3.7.2 Direct Correlation with Climate Drivers

To examine the factors influencing groundwater variability, long-term trends and non-seasonal anomalies in climate variables were analyzed, and the decomposition of climate data into Trend, Seasonal, and Residual components was performed with the Seasonal-Trend-Loess (STL) method [24] equation (3), where the climate anomaly signal was defined as the sum of the Trend and Residual components [19,30,31]. For this section, equation (3) consists of the original observed value of the climate variable at month t (Y_t), the value of the long-term Trend component at month t (T_t), which represents the slow-moving, multi-year variability and any underlying linear trend, and the seasonal component for month t (S_t), reflecting the predictable and cyclical trend within a year (such as wet and dry seasons). In the meantime, Rt represents the residual component for month t, which corresponds to the non-systematic irregularities, commonly referred to as noise or short-term events that are not captured by the trend or seasonal cycle.

2.3.7.3. Groundwater Response Tracers for Climate Indices

To validate the reality of GWSA and further investigate the influence of large-scale climate teleconnections, two independent climate indices were used.

The ONI is defined as a 3-month running mean of sea surface temperature anomalies in the Niño 3.4 region of the equatorial Pacific. Standard thresholds of ONI $\geq +0.5°C$ for El Niño and $\leq -0.5°C$ for La Niña were the baseline, and this index is a standard for identifying major ENSO events known to impact African rainfall [32,33], which can be related to the long-term dynamics of GWSA trend at continental scale. It is important to investigate the link between temperature and groundwater storage because precipitation deficits on water resources are dynamic due to rising temperatures [34], and hence the direct plot relationship analysis between GWSA and temperature was performed for further confirmation of the dynamic long-term trend of GWSA at continental scale.

2.3.8. Validation of GWSA and Recharge at Regional and Continental Scales

Access to observation data at regional and continental scales is challenging, particularly in Africa, where data recording and storage systems are poorly organized; therefore, it is reasonable to use disseminated and model outputs to compare consistency. As a result, estimating groundwater recharge remains a challenge and has motivated two distinct approaches in recent literature. The 134 recharge estimates were compiled by [4] and then upscaled statistically using a linear mixed model with constraints based on long-term average rainfall, resulting in a continental mean of ~49 mm yr^{-1} but excluding focused recharge from rivers, lakes, and irrigation return flow, and humid high recharge regions of the continent such as the Congo Basin and coastal and West Africa that dominate the continental water balance. More recently, [16] used an Ensemble Kalman Filter to assimilate TWS anomalies from GRACE, which resulted in a significantly larger mean continental recharge of ~173 mm yr^{-1}. Importantly, neither study checked the validity of model-recharge estimates using an independent dataset or in-situ network, with the first relying on model diagnostics to select recharge [4] and the second explicitly stating that in-situ data for groundwater was unavailable; checking against the internal consistency of the noise from the two GRACE disaggregation methods was used [16]. Considering this missing link in the existing literature and the significant differences between the two global estimates in the literature (of about 3.5-fold), we correlated the regional and continental GRACE-derived recharge with the WHYMAP transboundary aquifer recharge classification to define the limits of our estimates and what part is well constrained.

To validate the results of this comparison with the WHYMAP classification, regional and continental recharge estimates were also compared with ground-based recharge estimates from MacDonald [4], which were aggregated to the same 5 UN M49 sub-regions. Close agreement was seen for West and Middle Africa (ratios of 1.12 and 1.14, respectively), and greater but consistent differences were noted for East (1.79×), South (2.61×), and North Africa (9.7×). The relative spatial pattern reported here was the same when using both independent datasets, with North having the lowest ranking and Middle the highest ranking of recharge magnitude (distinct from the GWSA trend ranking above, where East Africa was highest). The large difference in North Africa is consistent with MacDonald [4] omitting certain recharge mechanisms such as wadi recharge and ephemeral river recharge, which are typically important in hyper-arid fossil-aquifer recharge but are included in the GRACE-based water-balance approach employed in this study.

The estimated of the continent (94.0 mm yr^{-1}) in the recharge between of the recent previous research works, 49 mm yr^{-1} [4] and 173 mm yr^{-1} [16], which falls within the uncertainty range of previous continental estimates.

Fig. 2 shows the GRACE-derived recharge against the WHYMAP hydrogeological classification for the continental aggregate (**Fig. 2a**), and for the five sub-regions of Africa (**Fig. 2 b–f**) with the corresponding Spearman rank correlation (ρ) for each. At the continental scale (**Fig. 2a**), the GRACE-derived recharge is statistically significantly correlated with WHYMAP class (ρ = 0.76, n = 43,650) and consistently increases from Class 11 (very low) through Class 15 (very high) in major basins, from Class 22 through Class 25 in complex-structure basins, and from Class 33 to Class 34 in local/shallow aquifers. The absolute recharge values in the low-productivity classes are higher than WHYMAP's nominal classes; however, the relative recharge values agree with the expected relative ordering across all three WHYMAP structural categories.

It is worth noting that for the WHYMAP correlation analysis, the numbers of 0.25° grid cells (n = 4,075–43,650) reported are not independent statistical observations but the number of 0.25° grid cells that were compared. Because the native resolution of the underlying GRACE mascon solution is ~300 km, neighboring grid cells are not independent but rather are spatially autocorrelated; consequently, the number of effective samples is much less than the number of grid cells for formal significance testing. The Spearman correlation coefficients (ρ) are then considered here as descriptive statistics that describe the strength and direction of the association between GRACE-derived recharge and WHYMAP classification, instead of as formally independent statistical tests at the given nominal n.

Western Africa had the best regional agreement (ρ = 0.80, n = 8,766; **Fig. 2b**), with the recharge increasing sharply and near-monotonically from Class 11 (~50 mm yr^{-1}) to Class 15 (~195 mm yr^{-1}), the highest-class separation of any region.

Eastern Africa (ρ = 0.67, n = 9,948; **Fig.2c**) also had a strong positive correlation between recharge and class, though with a noticeable inversion between Classes 23 and 24 where the median recharge for Class 24 (complex structures, high) was significantly higher and more variable than the adjacent major-basin classes. Weaker, though still significant, correlations were found in North Africa (ρ = 0.35, n = 11,646; **Fig. 2d**), Middle Africa (ρ = 0.34, n = 9,210; **Fig. 2e**), and South Africa (ρ = 0.31, n = 4,075; **Fig. 2f**). Partly because of the highest interquartile range for Class 13 (major basins, medium) at the basin level (about 67–99 mm yr^{-1}) which overlaps significantly with

the nominally higher productivity Class 24, the weaker relationship is found in Northern Africa. For the mid-range classes (13–15 and 23–24), middle Africa showed relatively short separation ranges, and interquartile ranges overlapped because of a more uniform recharge regime (humid tropical), reducing WHYMAP's discriminatory power. However, the weakest correlation and fewest classes represented (6 of the nine continental classes) were obtained for South Africa, which is likely due to the more arid climate and lower recharge rate of the region as well as the small sample density of the WHYMAP data (n = 4,075, the lowest of the five regions). Across the continent and the regions, the interquartile ranges were narrowest and the medians lowest for the low productivity classes (11, 22), whereas the high productivity classes (15, 24, 25, 34) had larger interquartile ranges and also higher medians, indicating that there was more variation in the humid, high-recharge zones. The few values that appeared for class 25 (complex structures, very high) occurred only in Middle and Eastern Africa and were characterized by narrow, high-value boxes (~145–160 mm yr^{-1}), reflecting its rarity and specificity as a classification.

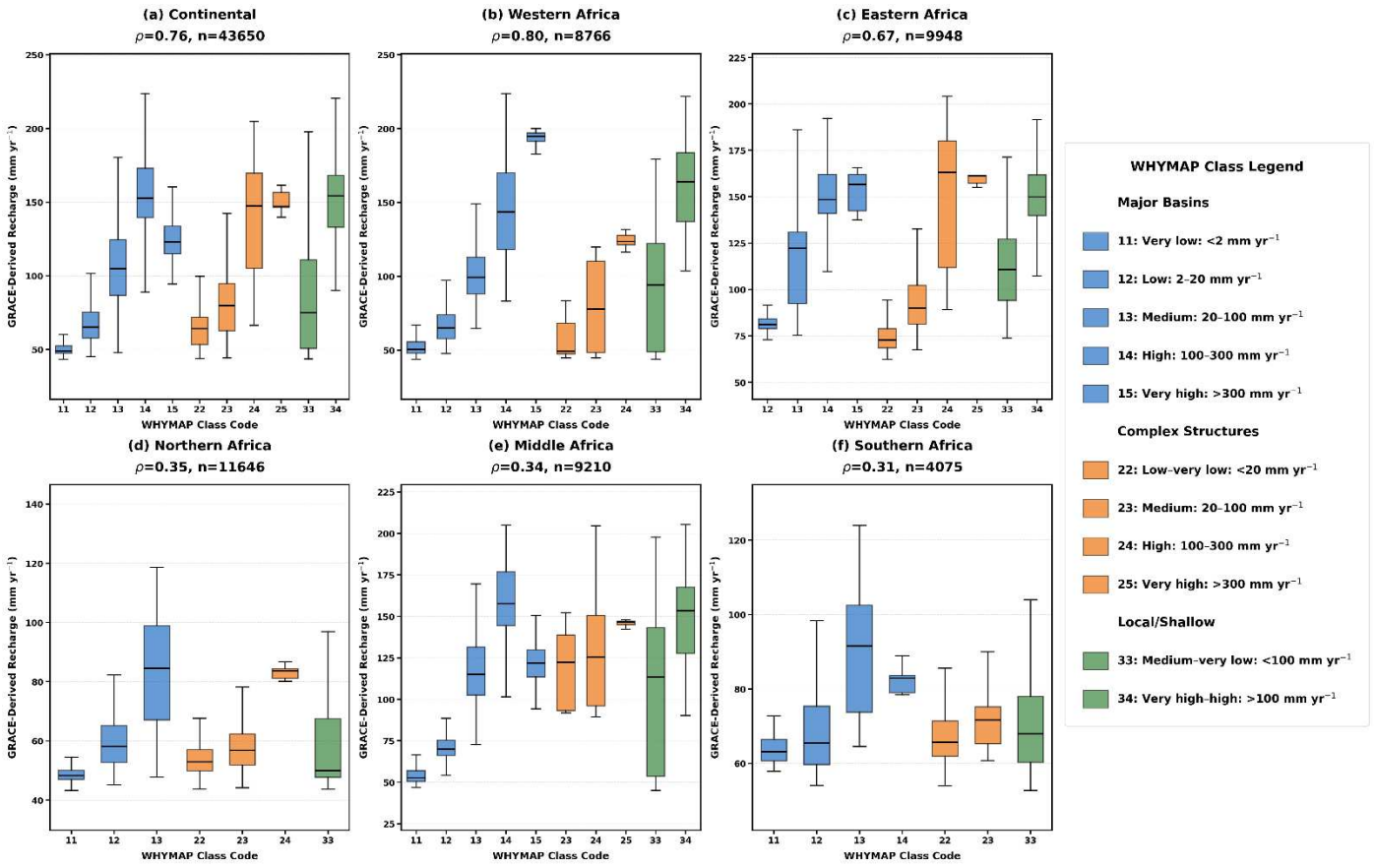


Fig. 2. Recharge Comparison with WHYMAP Recharge; (a) Continental (b) WA (c) EA (d) NA (e) MA (f) SA.

3. Results

The study area and processing framework (**Fig. 1**) provide the foundation for the groundwater storage estimates, and the climate-groundwater interaction presented in this study is scaled up from GRACE grid cells to the five sub-regions of Africa and the continent, thereby providing context for the results presented below.

3.1. Long-term Regional and Continental Trend of Groundwater Storage Anomaly

The continental GWSA has steadily risen since 2007, with a significant ramp-up after 2018-2020 (**Fig. 3a**), with a linear trend of 3.84 mm yr^{-1}. The continental mean GWSA time series exhibited a smooth upward trend but did not capture the interannual variability observed in the precipitation

time series. In comparison, the continental GWSA trend (3.84 mm yr^{-1}) was significantly larger than the continental precipitation trend (+0.10 mm yr^{-1}) (**Fig. 3a**).

The structural shift of the monthly GWSA time series over the entire continent is visible in the series of the turning point between the two linear trend regimes (**Fig. 3a**), significant in July 2020, and the increase in the slope of the GWSA trend is shifted from +2.59 mm yr^{-1} to +5.74 mm yr^{-1}. This transition was near the beginning of the extended, record-breaking La Niña, which began in 2020 and is projected to continue through 2022 and 2023 (**Fig. 7b**). Interestingly, the trend in precipitation was very much reduced beyond this breakpoint, despite a large increase in GWSA in the same time interval, from +0.10 to +0.01 mm yr^{-1}, which implies that more groundwater was stored after 2020 than what would be expected if total precipitation were the only factor of groundwater change, and that more storage could be occurred due to changes in rainfall intensity, timing, which increase the of groundwater recharge (**Fig. 6b**) during the 2020–2023 La Niña event, in addition to the reduction in groundwater abstraction (**Fig. 8b**).

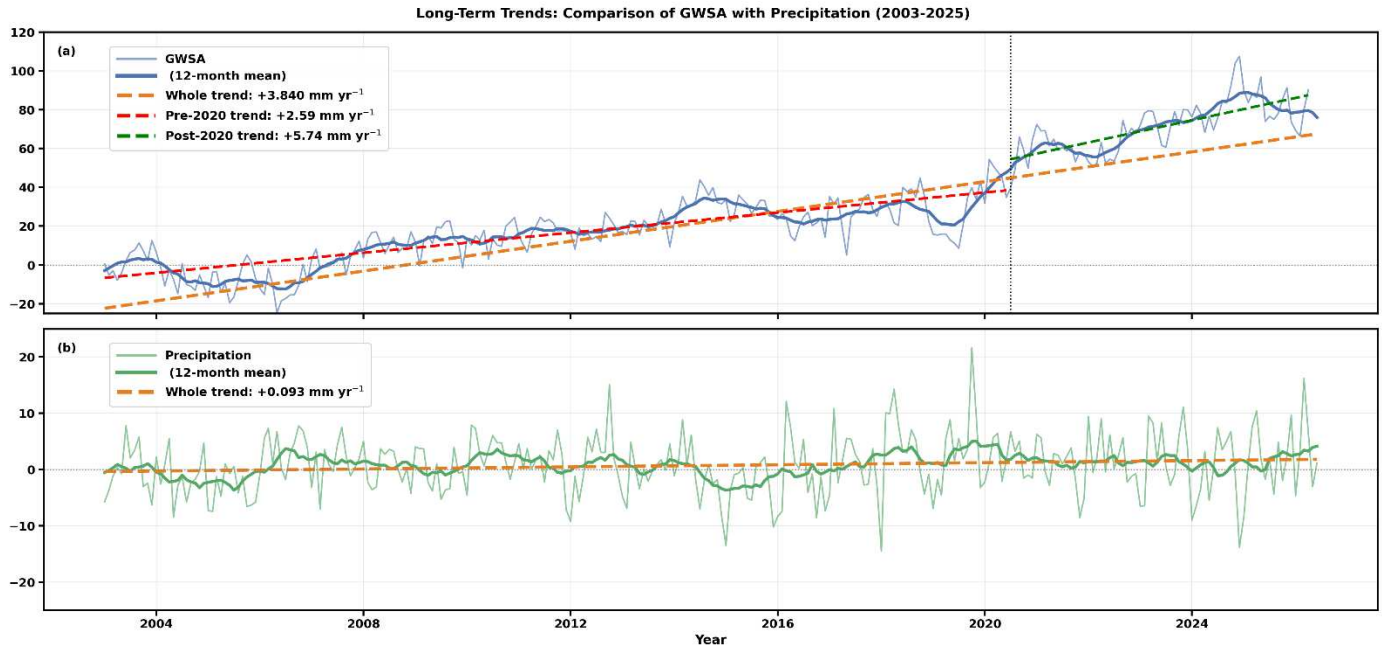


Fig. 3. Long-term monthly trend of GWSA with and without precipitation (mm yr^{-1}): a) GWSA; b) Precipitation from CHIRPS

When viewed at a regional level, the GWSA trends varied from −0.78 mm yr−1 in Northern Africa to +6.04 mm yr−1 in Eastern Africa, with positive trends of 5.27, 5.12, and 4.67 mm yr^{-1} for West,

Middle, and South Africa, respectively (**Fig. 4**), where precipitation trends range from +0.01 mm yr^{-1} (North Africa) to +0.21 mm yr^{-1} (East Africa).

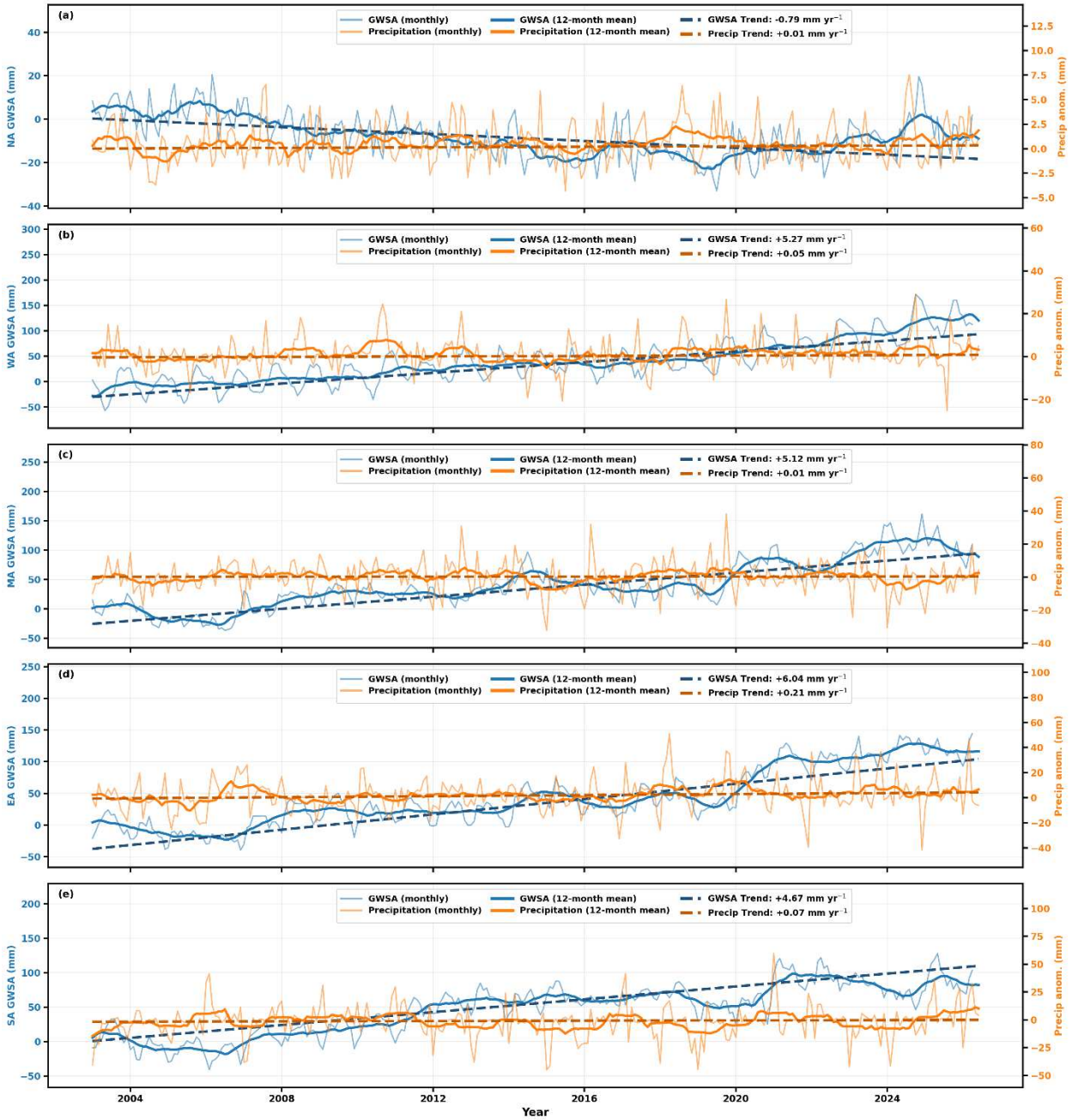


Fig. 4. Regional-scale trend relationship between GWSA and Precipitation

3.2. Spatial Variability of GWSA and Recharge Across African Regions

The mean monthly GWSA trend in the study time window (January 2003 to April 2026) declined in North Africa, whereas it increased in the other regions at a variable rate (**Fig. 5a)**. Regionally, the mean annual groundwater recharge indicates a signal in West, Central, and East Africa, such as over the Congo Basin and the West African coastal regions, and lower in the Sahara and northern Sahel (**Fig. 5b**).

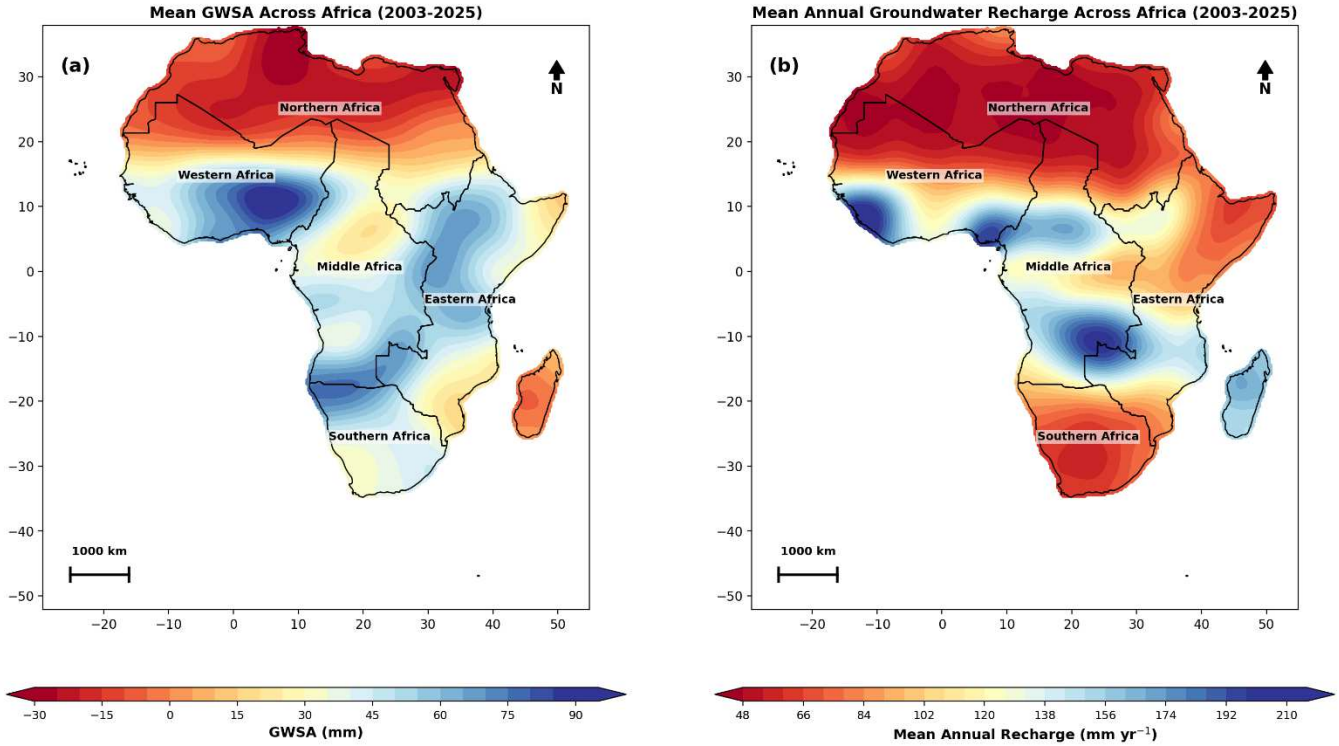
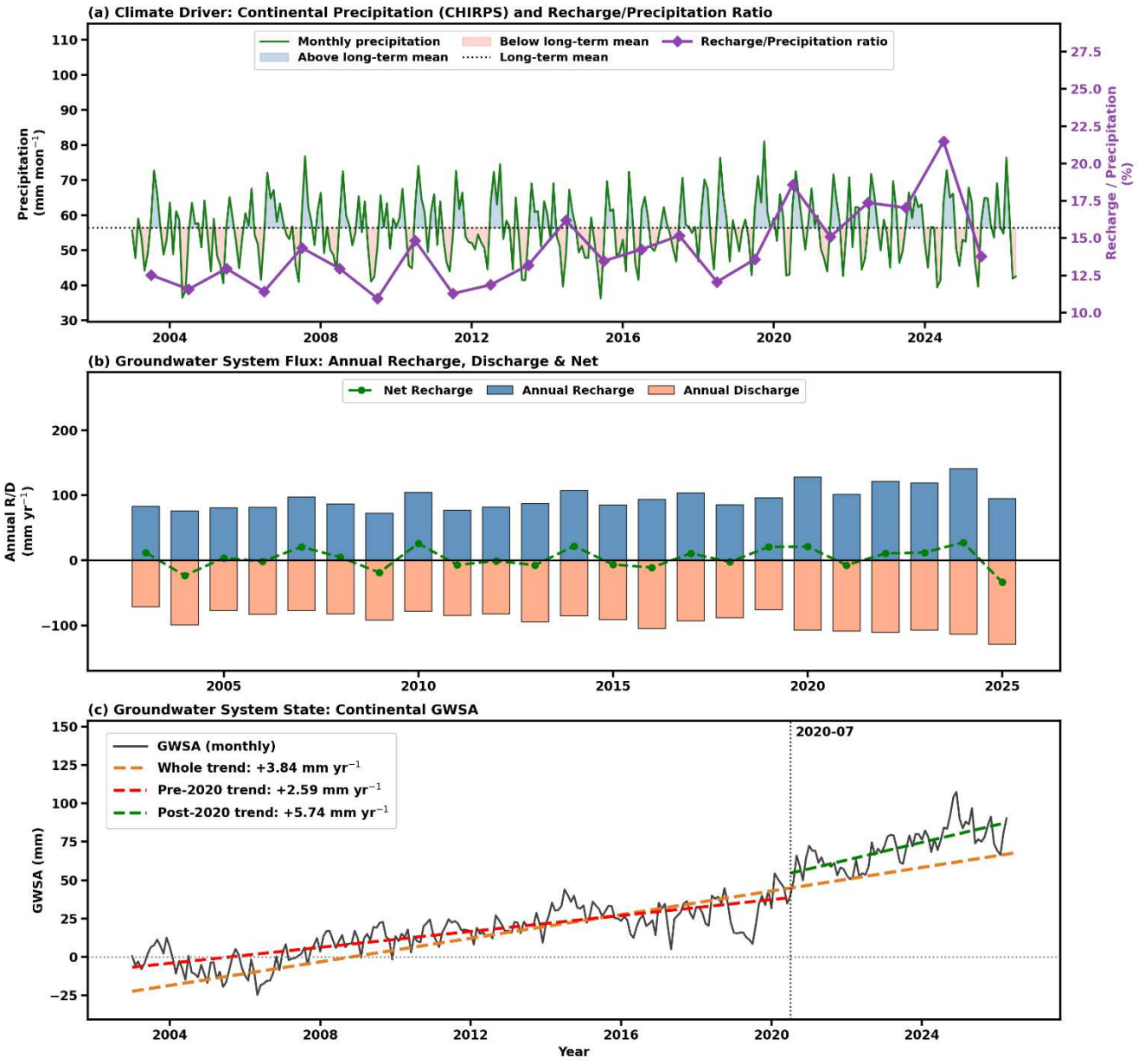


Fig. 5. Spatial variability of GWSA and recharge across the Regions

3.3. Precipitation, recharge, and storage relationships at continental scale

Continental precipitation showed monthly variability and low long-term variability (**Fig. 3b**), and net groundwater recharge remained near small positive values on average and exceeded discharge in most years (**Fig. 6b**).



321

322 **Fig. 6. Continental temporal variability: comparison of precipitation with GWSA and**
323 **recharge** (a) Recharge to precipitation ratio; (b) Groundwater recharges and discharges with net
324 recharge; (c) Continental GWSA (storage response)

325 **3.4. Climate Variable Anomalies and Teleconnections**

326 The correlation of GWSA and potential climate drivers at the continental scale indicates a small
327 positive long-term trend in continental temperature around +0.02 °C yr−1 while GWSA has a strong
328 positive trend of 3.84 mm yr−1 (two months dropped) for the entire study period (**Fig. 7a**). Likewise,

short-term changes in the Oceanic Niño Index (ONI) are correlated with changes in GWSA, as El Niño events are followed by short periods of groundwater storage loss and La Niña events by short periods of groundwater storage gain (**Fig. 7b**).

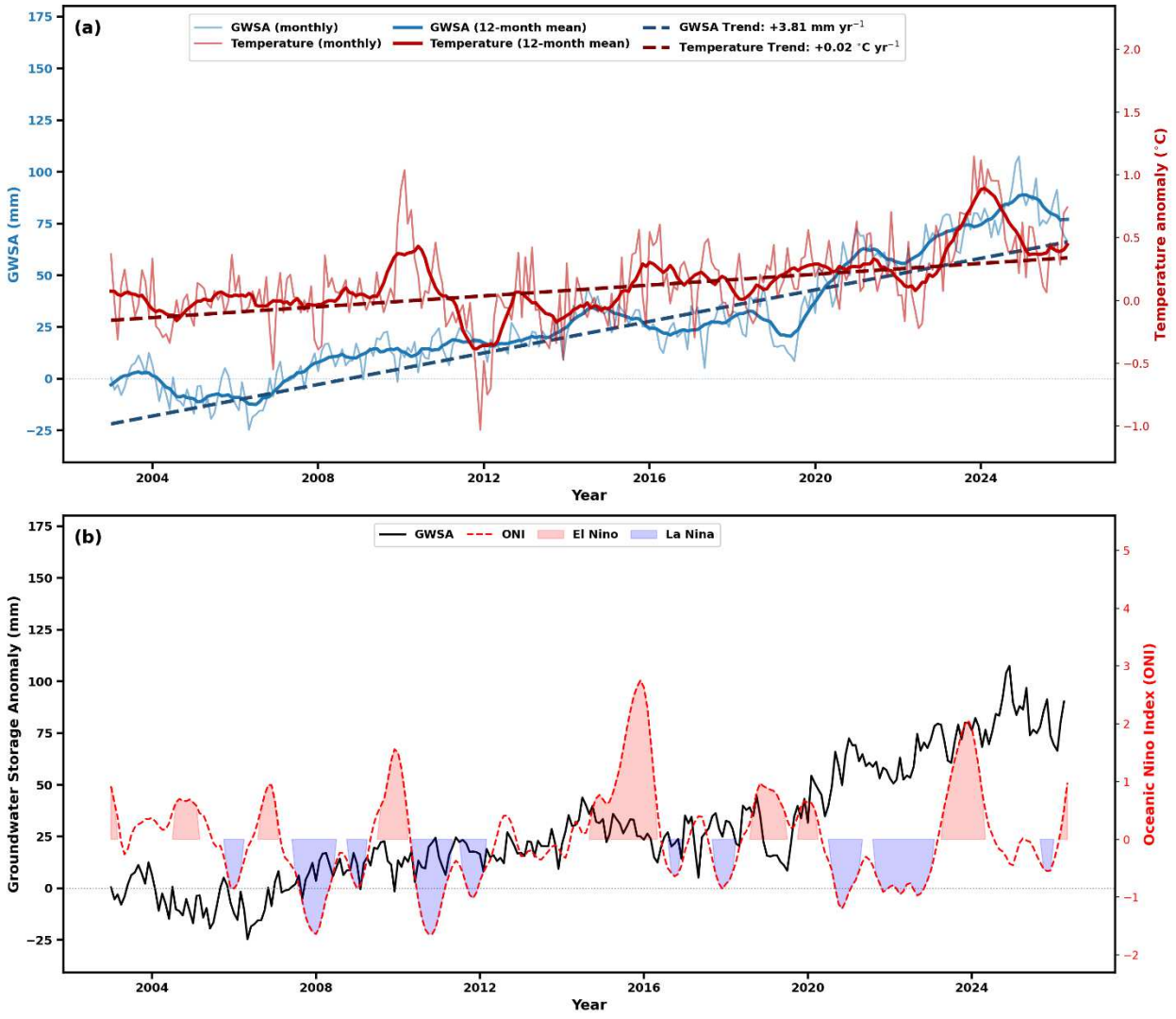


Fig. 7. Continental-scale comparison of GWSA with major Climate Events: (a) Continental GWSA and Temperature Anomalies; (b) Continental GWSA and Oceanic Niño Index (red) with both El Niño and La Niña episodes shaded, with no obvious ENSO-phase relationship with the post-2020 storage acceleration.

Nevertheless, the trend of GWSA remains positive, especially since 2020, with these climate oscillations, and hence the observations indicate that although temperature anomalies and ENSO-

related variations affect short-term groundwater storage changes, they are not linked to long-term changes in GWSA. Hence, the groundwater storage accumulation over time seems to be caused by a long-term imbalance between renewable groundwater resources and groundwater extraction (**Fig. 8**). The trends in precipitation have little variation +0.10 mm yr−1 and the GWSA trends (+3.84 mm yr−1 can emphasize multi-year climate cycles, damp memory, or large-scale water storage redistribution and not just year-to-year precipitation. As with all other GWSA, the gravity trend is not a direct indicator of a rising rainfall trend but may instead reflect more surface water pools, wetland expansion, or artificial reservoirs filling [10]. Furthermore, continental analysis comprises highly contrasting hydro-climatic zones, such as the hyper-arid Sahara and the humid Congo Basin, which would lead to a high degree of smoothing in the continental solution [16].

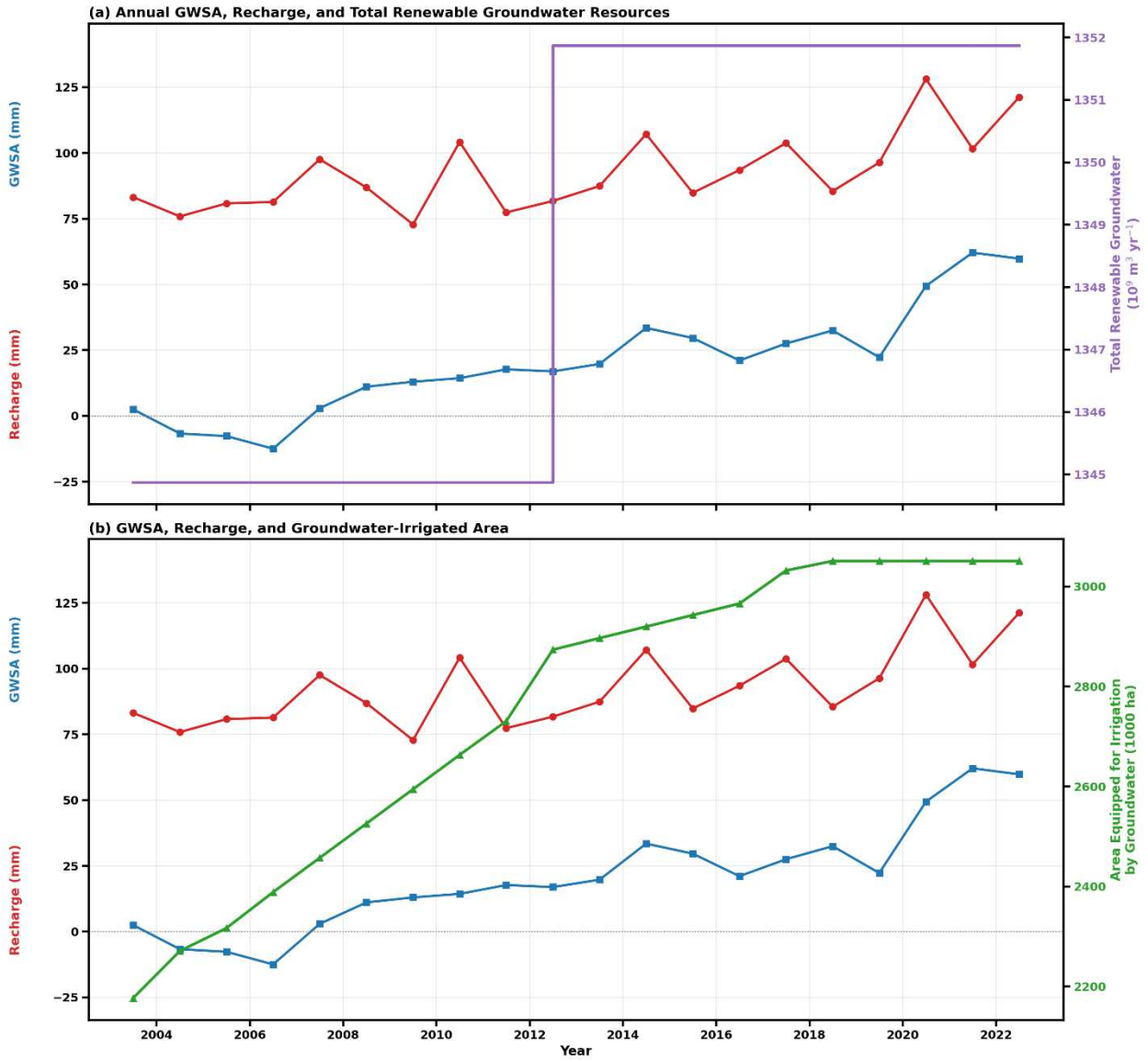


Fig. 8. Technical evidence for continental-scale upward trend of GWSA

(a) Annual Trend of GWSA, recharge and annual renewable groundwater resources (2003–2022); (b) Annual Trend of GWSA, recharge, and Percentage of irrigated area equipped by groundwater per 1000 ha

4. Discussion

4.1. Groundwater as the Dominant Component of Regional and Continental Water Storage Variability

The GWSA trend from this study shows continentally, GWSA is the most prominent contributor to the Africa continental TWS dynamics, where the trend of GWSA is 3.84 mm yr^{-1} at a continental scale (**Fig. 3a**), that is broadly similar to the strongest positive continental GWSA trends across all five sub-regions ranging from -0.78 mm yr^{-1} (North Africa) to +6.04 mm yr^{-1} (East Africa) (**Fig. 4**), though there were significant differences among the sub-regions in terms of recharge intensity (**Fig. 5b**). The analysis of this study indicates that the long-term trend of groundwater storage anomaly is almost the same as the trend of terrestrial water storage anomaly, exhibiting a strong rise since 2018, where anomalies of the other water storage components in the water balance equations of GRACE, however, are relatively small and highly stable. This finding provides powerful, continental- and regional-scale observational evidence that, over seasonal to decadal timescales, the variability of TWS observed from space over Africa primarily reflects water moving into and out of its vast subsurface aquifers. This is consistent with global syntheses, which show aquifer systems contain and are affected by the climate signal over multi-year timescales, but it is masked by short-term noise [35]. Furthermore, this work shows that groundwater buffering capacity depends strongly on continental scales. The signals appear stable, whereas at basin scales, heterogeneities may reflect rapid groundwater depletion in a stressed system [36]. Notably, the deep groundwater reservoir reflects delayed, cumulative expression of the much wetter conditions of 2018–2019.

4.2. Regional Dynamics of GWSA and Recharge in Africa

The continent-wide spatial patterns of mean GWSA and mean annual recharge (**Fig. 5**) show a clear north–south asymmetry that is generally similar across both variables but also emphasizes the relative importance of recharge magnitude and changes in long-term storage. The only region showing an obvious negative mean GWSA anomaly is over northern Africa, with values of around −30.6 mm during the study period (**Fig. 5a**), consistent with the lowest mean annual recharge for the continent (≲50–70 mm yr^{-1}; **Fig. 5b**) focused on the hyper-arid Sahara and northern Sahel regions. It is also physically consistent with the hydrogeology of the region, as much of the groundwater in Northern Africa is contained in non-renewable "fossil" aquifer systems such as the Nubian Sandstone and Northwestern Sahara Aquifer Systems, which receive limited recharge and are depleted primarily through sustained abstraction [16,37]. The near-zero recharge signal in **Fig. 5b** in this region therefore implies that any loss of GW will be irrecoverable on human timescales,

387 further confirming that the observed GWSA decline is not due to a recharge deficit caused by
388 climate change but rather reflects the mining of a largely non-renewable resource.

389 Conversely, the mean annual recharge is the greatest on the continent in the humid tropical belt
390 that stretches across coastal West Africa, such as the Guinea Highlands and the Congo Basin,
391 locally reaching more than 190–210 mm yr^{-1} (**Fig. 5b**), which corresponds to the highest
392 precipitation in this region driven by the ITCZ and the dense vegetation cover. Notably, this
393 recharge maximum does not necessarily correspond to the greatest positive GWSA anomaly (Fig.
394 5a), with Middle Africa showing a relatively small and spatially variable mean GWSA anomaly
395 compared with the consistently positive anomaly values over Eastern and South Africa, where
396 recharge is comparatively small. This decoupling highlights the following methodological point:
397 mean recharge is a flux term, which refers to the amount of water that enters the system over time,
398 while GWSA is a net balance of recharge and discharge (and anthropogenic abstraction) over time.
399 So, a region with high recharge can exhibit only a slight trend in storage if discharge (natural or
400 anthropogenic) is relatively high, and a region with moderate recharge can exhibit a strong positive
401 trend in storage if losses are relatively small, which is the case here when comparing Middle Africa
402 and Eastern and Southern Africa. The widespread GWSA positive anomalies over Western,
403 Middle, Eastern, and Southern Africa are consistent with the continent-wide wetting signal from
404 recent syntheses based on GRACE [38], whereas the isolated negative GWSA anomalies over
405 Northern Africa correspond to basin-based transboundary aquifer assessments [37]. These regional
406 trends, taken together, suggest that the nature of groundwater change in Africa is not uniform but
407 rather is a function of both climatically related recharge, which is dominant in the humid tropics,
408 and abstraction-related depletion, which is dominant in the arid north, which has important
409 implications for regional groundwater management strategies.

410 **4.3. Long-Term GWSA Trends and Post-2020 Hydro-Climatic Regime Shift**

411 The overall long-term trend regionally (**Fig. 4**) and continentally (**Fig. 3b**) indicates a significant
412 long-term increasing trend over the study period, with regional trend variation of -0.78 mm yr^{-1}
413 (North Africa) to 6.04 mm yr^{-1} (East Africa), whereas continentally the trend is 3.84 mm yr^{-1},
414 which is higher than the continental precipitation trend of 0.10 mm yr^{-1}. This indicates the long-
415 term positive precipitation anomalies with regional trend variation of 0.01 mm yr^{-1} (North Africa)

and 0.21 mm yr^{-1} (East Africa) (**Fig. 4),** contributed at episode precipitation time scale where GWSA records such climate effect as memory, and this noticed especially during the strongest recovery post 2020 period where the deep groundwater reservoir reflecting delayed, cumulative expression of the much wetter conditions of 2018–2019 (**Fig. 3a**; **Fig. 4**). The trend has distinct multi-year phases, from the beginning (2003) to the end (2025), of depletion, stability, and unprecedented replenishment where the GWSA reached about 85 mm by the end of 2025 at annual trend of 3.84 mm yr^{-1} even though the trend long trend of precipitation is 0.10 mm yr^{-1} for precipitation taken from CHIRPS. This finding is consistent with the established understanding that groundwater holds the largest portion of the planet's liquid freshwater [39]. The most notable evidence is a hydro-climatic regime shift since 2020 (Fig. 3a & b), where the GWSA average indicates long-term recharge, as shown by sharp changes in the Sahel through prolonged wet anomalies [3]. The high recharge pulses occurring after 2020 (**Fig. 6b**), consistent with earlier studies [16], are not only a temporary increase but could also be a sign of a transition of the continental system to a higher-storage regime; to confirm permanence, the high recharge would need to be sustained by another drought. This corresponds to new research suggesting an intensification of the African water cycle and re-vegetation in parts of the Sahel, which partially offset the severe droughts of the 1970s and 80s [3]. The rapid and sustained increase in these values indicates a high level of "resilience" in many African groundwater systems, that is, the potential for systems to respond markedly to a few years of above-average rainfall, as described earlier in [3].

4.4. Groundwater Response to Climate Variability

The annual groundwater recharge and discharge fluxes (**Fig. 6b**) have intermittent variations, which broadly co-vary with regional and continental precipitation (**Fig. 3a**; **Fig. 4b**), and in shorter cycles, with the phase of the El Niño–Southern Oscillation (ENSO) (**Fig. 7b**). The decline in the net recharge during the last decade (2015–2016; **Fig. 6b**) is associated with the strong El Niño event of 2015–2016 (**Fig. 7b**), aligning with reports of severe droughts during this period in Eastern and Southern African countries [40], and consistent with the large-scale evidence that ENSO teleconnections are one of the main drivers of hydro-climatic variability over the continent [32,41]. The corresponding transition towards positive net recharge, especially from 2020 to 2023 (**Fig. 6b**), and the upward trend of GWSA (**Fig. 3a**) are accompanied by La Niña becoming more frequent (**Fig. 7b**), which broadly mirrors the reported literature dipole relationship, where El Niño

is associated with drying in Southern Africa and often with opposing conditions over parts of East Africa [30]. However, groundwater storage anomalies (GWSA) and recharge rates do not respond immediately to ENSO but instead exhibit a lag, given the nature of groundwater systems. As a result, ENSO events and groundwater signals overlap chronologically over longer timescales. This covariation can serve as a long-term ENSO proxy; the multi-year evolution of GWSA reflects underlying ENSO variability and is directly sensitive to large-scale climate teleconnections during El Niño and La Niña years. Our findings also indicate an apparently sustained recharge increase, consistent with the annual recharge-discharge variation (**Fig. 6b**), which appears to result from a cumulative, longer-term imbalance between groundwater recharge and withdrawal (**Fig. 8**), in addition to a response to climate teleconnections.

4.5. Annual Renewable Groundwater Resources as Technical Evidence in Africa

Based on available data, the temporal evolution of groundwater-irrigated areas and groundwater contribution to irrigation water supply in Africa from 2003-2022 (**Fig. 8**) was used as technical evidence to justify the long-term increase in GWSA and recharge at the continental scale. Groundwater-supported irrigation expanded across Africa, with the groundwater-irrigated area steadily increasing between 2003 and 2018 (**Fig. 8b**), followed by stabilization thereafter. From the same database, it has been noted that groundwater withdrawals were relatively small compared to annual renewable groundwater resources, with an increase before 2012, but still lower than renewable groundwater resources for the entire period (**Fig. 8a**). A significant change after 2012 indicates that groundwater renewable resources rose significantly, whereas the groundwater-irrigated area coverage remained relatively constant with only minor changes. This resulted in a larger difference between groundwater renewable resources and groundwater abstraction for the post-2012 period, reflecting an increased tendency for groundwater replenishment higher than abstraction (**Fig. 8**). The conditions were like those of later years when groundwater storage anomaly increased, indicating that groundwater resource sustainability was provided by increased groundwater renewable resources.

4.6. Region-Specific Implications for Groundwater Management

The distinct regional differences in GWSA and recharge illustrated above suggest that regionally appropriate groundwater management strategies should be developed rather than applied across the continent.

In northern Africa, groundwater is drawn primarily from non-renewable “fossil” aquifer systems such as the Nubian Sandstone and Northwestern Sahara Aquifer Systems, where GWSA is

declining (−0.78 mm yr^{-1}) and recharge is negligible across the hyper-arid Sahara and northern Sahel. Strict abstraction limits based on transboundary agreements, increased monitoring of depletion, and investments in alternative sources of abstraction (desalination, treated wastewater reuse) to reduce dependence on this largely irrecoverable resource are priorities.

In western and Middle Africa, humid, high-recharge belts, such as the Congo Basin and coastal West Africa (locally >190–210 mm yr^{-1}), are associated with the greatest regional GWSA gains (+5.27 and +5.12 mm yr^{-1}, respectively). They should include protecting recharge areas from land use change and deforestation, managed aquifer recharge when possible, and scaling up the expansion of groundwater-fed irrigation to match recharge potential to avoid tomorrow's over-abstraction for today's surplus.

In eastern and southern Africa, average GWSA trends indicate moderate to positive changes (+6.04 and +4.67 mm yr−1, respectively), but they are susceptible to ENSO-related droughts, such as the 2015–2016 El Niño and the 2020–2022 Horn of Africa drought. Conjunctive-use planning and seasonal forecasting with ONI monitoring should be given high priority to mitigate the impacts of drought years on agriculture and water supply and to maintain the observed ability of these systems to rebuild after multi-year droughts.

If the abstraction rate of groundwater resources exceeds their supply at a continental scale, there is an opportunity for proactive governance to address the resulting gap. The in-situ groundwater networks need to be strengthened, and cross-border water data sharing needs to be improved and harmonized, while the use of GRACE-derived GWSA products in national water-resource assessments would help sustain evidence-based groundwater management in the face of increasing irrigation and urban demand across the continent.

5. Conclusion

This is the first continent-wide assessment of groundwater storage change in Africa using GRACE, spanning 2003 to 2025. To quantify the GWSA, the recharge and the discharge across the continent were determined using a 0.25° regular grid interpolation at monthly resolution, via mass-balanced disaggregation of the GRACE/GRACE-FO TWSAs, refined by the Ensemble Kalman Filter and validated with the WHYMAP groundwater recharge classification, and related to precipitation, temperature, and ENSO to characterize the sensitivity of African groundwater to these climate variables.

Continental GWSA has been increasing since 2007 and has accelerated significantly since 2018-2020, with values reaching approximately 85 mm at the end of 2025, with a trend of 3.84 mm yr^{-1}, much higher than the continental precipitation trend (+0.10 mm yr^{-1}), with continental recharge-to-precipitation ratio varying from 11.0% to 21.5%. The upward trend in GWSA across the continent is evident in renewable groundwater resources not depleted by abstraction during the study period. However, this was not a consistent pattern, with GWSA decreasing for most of Northern Africa (-0.78 mm yr^{-1}), largely due to the depletion in non-renewable fossil aquifers, and increasing strongly across Western, Middle, Eastern and Southern Africa (+4.67 mm yr^{-1} to +6.04 mm yr^{-1}), largely because of the high recharge in the humid tropics, and a post-2020 hydro-climatic regime shift where the trend of GWSA increased from 2.59 mm yr^{-} to 5.74 mm yr^{-} associated with an extended period of La Niña.

These regional differences have direct management implications, including conserving non-renewable reserves in the more arid northern areas and ensuring recharge-driven gains in the Western, Middle, Eastern, and Southern parts of the continent. In general, the findings indicate that continental GWSA is a strong, physically coherent proxy of Africa's groundwater response to climate variability and human abstraction, suggesting apparent recovery in storage over the last few years should not be considered a buffer against continued climate and demographic pressures: it will require ongoing monitoring, region-wide management, and evidence-based policy to sustain this resource. Moreover, changes in GWSA could alter surface latent and sensible heat fluxes, with downstream effects on boundary-layer soil moisture and cloud properties. A synergistic analysis linking land-surface fluxes, cloud microphysics, and GWSA could further clarify this hydroclimate and environmental feedback, a promising direction for future work.

Acknowledgement

We are very grateful to the Taiwan International Graduate Program (TIGP) for its financial assistance, which played an important role in completing this research. This work was supported by Academia Sinica under the grant number: AS-IAIA-114-M03, and Taiwan National Science and Technology Council under the grant numbers: NSTC 115-2116-M-008 -001, NSTC 115-MOEA-M-008 -001, NSTC 114-2116-M-008 -025, NSTC 115-2621-M-008 -003 -MY3, NSTC 114-2621-M-008 -004, NSTC 114-2740-M-001-002, NSTC 115-2111-M-001-010, and NSTC 115-2119-M-001-004.

Author Contribution

G.K.B. conceived the study, developed the methodology, performed data curation, formal analysis, and visualization, and wrote the original draft. C.-F.N. supervised the research; he contributed to the conceptualization and methodological design and reviewed and edited the manuscript. C.- Y.L. contributed to the validation and interpretation of the results and reviewed and edited the manuscript. Each author reviewed and approved the final manuscript.

Declaration of Competing Interests

The authors declare no competing interests

Data Availability

In this study, all external datasets are publicly available as summarized below:

1. Total Water Storage Anomaly (TWS) from GRACE/GRACE-FO (CSR RL0603 Mascons), University of Texas Center for Space Research (CSR):
https://download.csr.utexas.edu/outgoing/grace/RL0603_mascons/CSR_GRACE_GRACE-FO_RL0603_Mascons_all-corrections.nc
2. Soil moisture, snow water equivalent, canopy water storage, and evapotranspiration derived from the GLDAS-Noah model.
https://giovanni.gsfc.nasa.gov/giovanni
3. DAHITI lake water-level anomalies: Deutsches Geodätisches Forschungsinstitut, Technical University of Munich (registration is required): https://dahiti.dgfi.tum.de
4. Create polygon geometry for lakes from HydroLAKES:
https://www.hydrosheds.org/products/hydrolakes
5. CHIRPS precipitation: Climate Hazards Center, UC Santa Barbara:
https://www.chc.ucsb.edu/data/chirps
6. Reanalysis 2 m air temperature and the Oceanic Niño Index (ONI) — NOAA Climate Prediction Center: https://www.cpc.ncep.noaa.gov
7. World Administrative and Physical Boundaries: https://www.naturalearthdata.com
8. Groundwater Watcher: WHYMAP - WHYMAP - Groundwater Resources of Africa
9. Annual renewable groundwater and groundwater-irrigated area: FAO AQUASTAT Dissemination System

All the data sets generated and analyzed in this study, mainly GWSA, recharge and discharge datasets, and the processing and analysis, are available upon request from the corresponding author.

6. References

1 Taylor, R. G. *et al.* Ground water and climate change. *Nat. Clim. Change* **3**, 322–329 (2013). https://doi.org/10.1038/nclimate1744

2 Adeyeri, O. E. Hydrology and Climate Change in Africa: Contemporary Challenges, and Future Resilience Pathways. *Water* **17** (2025). https://doi.org/10.3390/w17152247

3 Cuthbert, M. O. *et al.* Global patterns and dynamics of climate–groundwater interactions. *Nat. Clim. Change* **9**, 137–141 (2019). https://doi.org/10.1038/s41558-018-0386-4

4 MacDonald, A. M. *et al.* Mapping groundwater recharge in Africa from ground observations and implications for water security. *Environ. Res. Lett.* **16** (2021). https://doi.org/10.1088/1748-9326/abd661

5 Pokhrel, Y. *et al.* Global terrestrial water storage and drought severity under climate change. *Nat. Clim. Change* **11**, 226–233 (2021). https://doi.org/10.1038/s41558-020-00972-w

6 Papa, F. *et al.* Water resources in Africa under global change: monitoring surface waters from space. *Surv. Geophys.* **44**, 43–93 (2023). https://doi.org/10.1007/s10712-022-09700-9

7 Roy, I., Mliwa, M. & Troccoli, A. Important drivers of East African monsoon variability and improving rainy season onset prediction. *Nat. Hazards* **120**, 429–445 (2024). https://doi.org/10.1007/s11069-023-06223-3

8 Scanlon, B. R. *et al.* Global models underestimate large decadal declining and rising water storage trends relative to GRACE satellite data. *Proc. Natl. Acad. Sci. U.S.A.* **115**, E1080–E1089 (2018). https://doi.org/10.1073/pnas.1704665115

9 Zhang, L. *et al.* Separating Climatic and Anthropogenic Drivers of Groundwater Change in an Arid Inland Basin: Insights from the Shule River Basin, Northwest China. *Remote Sens.* **17**, 3188 (2025). https://doi.org/10.3390/rs17183188

10 Scanlon, B. R. *et al.* Linkages between GRACE water storage, hydrologic extremes, and climate teleconnections in major African aquifers. *Environ. Res. Lett.* **17** (2022). https://doi.org/10.1088/1748-9326/ac3bfc

11 Magaji Ibrahim, M., Ibrahim, M. & Mubi Aisha, M. Groundwater storage variability in West Africa using gravity recovery and climate experiment (GRACE) and global land data assimilation system (GLDAS) data. *EQA-Int. J. Environ. Qual.* **64**, 87–102 (2024). https://doi.org/10.6092/issn.2281-4485/20167

12 Gaye, C. B. & Tindimugaya, C. Review: Challenges and opportunities for sustainable groundwater management in Africa. *Hydrogeol. J.* **27**, 1099–1110 (2018). https://doi.org/10.1007/s10040-018-1892-1

13 Tapley, B. D., Bettadpur, S., Ries, J. C., Thompson, P. F. & Watkins, M. M. GRACE Measurements of Mass Variability in the Earth System. *Science* **305**, 503–505 (2004). https://doi.org/10.1126/science.1099192

14 Rodell, M. *et al.* The global land data assimilation system. *Bull. Am. Meteorol. Soc.* **85**, 381–394 (2004). https://doi.org/10.1175/BAMS-85-3-381

15 Yi, S. & Sneeuw, N. Filling the data gaps within GRACE missions using singular spectrum analysis. *J. Geophys. Res. Solid Earth* **126**, e2020JB021227 (2021). https://doi.org/10.1029/2020JB021227

16 Ferreira, V. G. *et al.* Estimating groundwater recharge across Africa during 2003–2023 using GRACE-derived groundwater storage changes. *J. Hydrol. Reg. Stud.* **56**, 102046 (2024). https://doi.org/10.1016/j.ejrh.2024.102046

17 Tapley, B. D. *et al.* Contributions of GRACE to understanding climate change. *Nat. Clim. Change* **5**, 358–369 (2019). https://doi.org/10.1038/s41558-019-0456-2
18 Schwatke, C., Dettmering, D., Bosch, W. & Seitz, F. DAHITI – an innovative approach for estimating water level time series over inland waters using multi-mission satellite altimetry. *Hydrol. Earth Syst. Sci.* **19**, 4345–4364 (2015). https://doi.org/10.5194/hess-19-4345-2015
19 Welch, G. & Bishop, G. An introduction to the kalman filter (Tech. Rep. No. 95-041). *Chapel Hill, NC: University of North Carolina* (2004).
20 Messager, M. L., Lehner, B., Grill, G., Nedeva, I. & Schmitt, O. Estimating the volume and age of water stored in global lakes using a geo-statistical approach. *Nat. Commun.* **7**, 13603 (2016). https://doi.org/10.1038/ncomms13603
21 Funk, C. *et al.* The Climate Hazards Center Infrared Precipitation with Stations, Version 3. *Sci. Data* **13** (2026). https://doi.org/10.1038/s41597-026-07096-4
22 Bundesanstalt für Geowissenschaften und, R., United Nations Educational, S. & Cultural, O. (BGR and UNESCO, Berlin; Paris, 2018).
23 Cao, Y., Ge, G., Bao, Y., Chang, A. & Niu, R. Study on the Changing Trend of Terrestrial Water Storage in Inner Mongolia Based on GRACE Satellite and GLDAS Hydrological Model. *Water* **17** (2025). https://doi.org/10.3390/w17213123
24 Cleveland, R. B., Cleveland, W. S., McRae, J. E. & Terpenning, I. STL: A Seasonal-Trend Decomposition Procedure Based on Loess. *J. Off. Stat.* **6**, 3–73 (1990).
25 Sharifi, E., Haas, J., Boergens, E., Dobslaw, H. & Güntner, A. Technical note: GRACE-compatible filtering of water storage data sets via spatial autocorrelation analysis. *Hydrol. Earth Syst. Sci.* **29**, 6985–6998 (2025). https://doi.org/10.5194/hess-29-6985-2025
26 Save, H., Bettadpur, S. & Tapley, B. D. High-resolution CSR GRACE RL05 mascons. *J. Geophys. Res. Solid Earth* **121**, 7547–7569 (2016). https://doi.org/10.1002/2016JB013007
27 Ma, Y. *et al.* Improved estimates of sub-regional groundwater storage anomaly using coordinated forward modeling. *Water Resour. Res.* **60**, e2023WR036105 (2024). https://doi.org/10.1029/2023WR036105
28 Zhang, J., Hu, L., Sun, J. & Wang, D. Reconstructing groundwater storage changes in the North China Plain using a numerical model and GRACE data. *Remote Sens.* **15**, 3264 (2023). https://doi.org/10.3390/rs15133264
29 Richey, A. S. *et al.* Quantifying renewable groundwater stress with GRACE. *Water Resour. Res.* **51**, 5217–5238 (2015).
30 Chin, S. *et al.* VISTA: A training-free unsupervised algorithm for time series anomaly detection. *Patterns* **6**, 100789 (2025). https://doi.org/10.1016/j.patter.2025.100789
31 Aslam, M. & Ullah, M. I. *Practicing R for statistical computing*. (Springer, 2023).
32 Kolusu, S. R. *et al.* The El Niño event of 2015–2016: climate anomalies and their impact on groundwater resources in East and Southern Africa. *Hydrol. Earth Syst. Sci.* **23**, 1751–1762 (2019). https://doi.org/10.5194/hess-23-1751-2019
33 Mpheshea, L. E., Blamey, R. C. & Reason, C. J. The influence of ENSO-type on rainfall characteristics over Southern Africa during the austral summer. *Clim. Dyn.* **63**, 1–24 (2025). https://doi.org/10.1007/s00382-024-07489-4
34 Yin, D., Li, Q., Li, X. & Zhu, R. Annual water deficit in response to climate variabilities across the globe. *Environ. Res. Lett.* **17** (2022). https://doi.org/10.1088/1748-9326/ac5d9b

35 Williams, A. P. *et al.* Large contribution from anthropogenic warming to an emerging North American megadrought. *Science* **368**, 314–318 (2020). https://doi.org/10.1126/science.aaz9600
36 Jasechko, S. *et al.* Rapid groundwater decline and some cases of recovery in aquifers globally. *Nature* **625**, 715–721 (2024). https://doi.org/10.1038/s41586-023-06879-8
37 Frappart, F. Groundwater Storage Changes in the Major North African Transboundary Aquifer Systems during the GRACE Era (2003–2016). *Water* **12** (2020). https://doi.org/10.3390/w12102669
38 Hohensinn, R. *et al.* Water storage trends derived from the GRACE/-FO global gravity-based groundwater product (G3P). *EGUsphere* (2026). https://doi.org/10.5194/egusphere-2026-975
39 Gleeson, T., Befus, K. M., Jasechko, S., Luijendijk, E. & Cardenas, M. B. The global volume and distribution of modern groundwater. *Nat. Geosci.* **9**, 161–167 (2015). https://doi.org/10.1038/ngeo2590
40 Gebremeskel Haile, G. *et al.* Droughts in East Africa: Causes, impacts and resilience. *Earth Sci. Rev.* **193**, 146–161 (2019). https://doi.org/10.1016/j.earscirev.2019.04.015
41 Ascott, M. J. *et al.* Time of emergence of impacts of climate change on groundwater levels in sub-Saharan Africa. *J. Hydrol.* **612** (2022). https://doi.org/10.1016/j.jhydrol.2022.128107